JOC The Journal of Organic Chemistry

Article

pubs.acs.org/joc

Theoretical Insight into the Mechanisms and Regioselectivity of [4 + 3] and [4 + 1] Annulations of Enals with Azoalkenes Catalyzed by N-Heterocyclic Carbenes

Tao Liu,[†] Shumin Han,[‡] Yaping Li,[‡] and Siwei Bi*[,‡]

[†]Department of Chemistry and Chemical Engineering, Jining University, Qufu 273155, Shandong Province, People's Republic of China

[‡]School of Chemistry and Chemical Engineering, Qufu Normal University, Qufu 273165, Shandong Province, People's Republic of China

Supporting Information

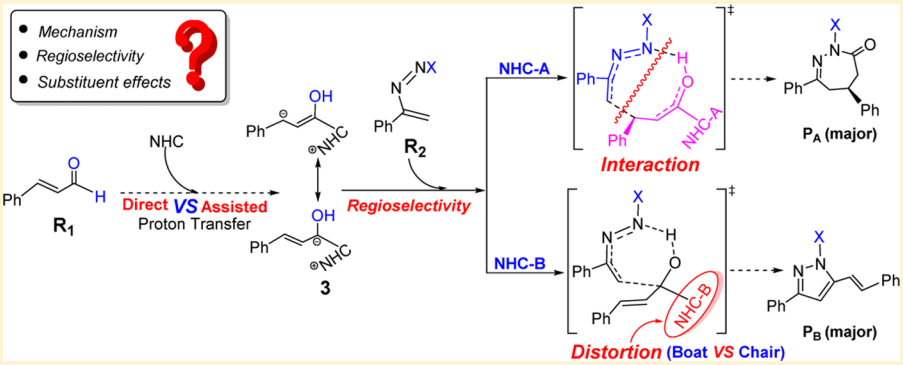

ABSTRACT: The reaction mechanisms on the NHC-catalyzed [4 + 3] and [4 + 1] annulations of enals with azoalkenes have been theoretically investigated with the aid of the density functional theory calculations. It is found that the additives play an important role in promoting proton transfer and dehydration. The impacts of catalysts (**NHC-A** and **NHC-B**) and substituent groups on the regioselectivity were rationalized. The origin of the regioselectivity involved in these reactions was probed by performing distortion−interaction analysis. For reaction A with **NHC-A** as the catalyst and Boc group as the substituent, the regioselectivity is predicted to be determined by the interaction energy of **3** with $\mathbf{R_2}'$ in $\mathbf{TS_3}^{A}$ versus $\mathbf{TS_8}^{A}$. For reaction B with **NHC-B** as the catalyst and Boc group as the substituent, the unstable boat-type conformation versus the stable chair-type conformation involved in the **NHC-B** moiety accounts for the regioselectivity. In reaction C with **NHC-A** as the catalyst and Ts group as the substituent, distortion energies of **3** and $\mathbf{R_2}'$ in $\mathbf{TS_3}^{C}$ versus $\mathbf{TS_6}^{C}$ are found to be the major reason delivering regioselectivity even higher than that of reaction A.

INTRODUCTION

Due to the depressant, antimicrobial, and antiviral activity, important biologically active compounds, diazepines[1−3] and pyrazole derivatives,[4−6] have been widely used in the pharmaceutical and agrochemical industries. However, lack of synthesis methods and complication of synthesis processes limited preparation of these products. As one unique class of organocatalysts, N-heterocyclic carbenes (NHCs) have attracted more and more attention because of their hypotoxicity, stability, and nucleophilic ability of carbenes.[7−11] In recent years, a series of NHC-catalyzed cycloaddition reactions generating different heterocycles were reported, including [3 + 2],[12−15] [2 + 2],[16,17] [4 + 2],[18,19] and [4 + 3][20,21] cycloadditions.

Very recently, Glorius et al. reported NHC-catalyzed formal [4 + 3] and [4 + 1] annulation reactions, delivering 1,2-diazepines and pyrazoles with good chemo- and regioselectivity (Scheme 1).[22] As shown in Scheme 1, two different substrates, enals ($\mathbf{R_1}$) and hydrazone ($\mathbf{R_2}$), could produce two possible products, $\mathbf{P_A}$ or $\mathbf{P_B}$, via annulation reactions in the presence of the NHC precatalysts **A** (**NHC-A**) or **B** (**NHC-B**). Catalyst **NHC-A** involves a chiral triazolium with 2,4,6-$Me_3C_6H_2$, and catalyst **NHC-B** involves an amorpholine backbone with 2,6-$(OMe)_2C_6H_3$. When the substituent **X** in $\mathbf{R_2}$ is a Boc group, experiments demonstrated that the product ratios of $\mathbf{P_A}/\mathbf{P_B}$ are 9:1 with **NHC-A** and <1:20 with **NHC-B** as the catalyst. With **NHC-A** as the catalyst and Ts as the substituent, the product ratio of $\mathbf{P_A}/\mathbf{P_B}$ is increased to >20:1. To account for the distinct regioselectivity, the Glorius group postulated possible reaction mechanisms that are summarized in Scheme 2. First, nucleophilic addition of **NHC-A** (or **NHC-B**) to the aldehydic carbon of $\mathbf{R_1}$ gives a zwitterionic intermediate **A1** (or **B1**). Second, the 1,2-proton transfer generates the extended Breslow intermediate **A2** (or **B2**). Third, azoalkene $\mathbf{R_2}'$, formed in situ from substrate $\mathbf{R_2}$ through HCl elimination, undergoes homoenolate 1,4-addition or acyl anion 1,4-addition to form a new carbon−carbon σ bond, giving intermediate **A3** (or **B3**). Fourth, 1,6-proton transfer generates intermediate **A4** with the nitrogen atom bearing a negative charge.

Received: July 29, 2016
Published: September 28, 2016

ACS Publications © 2016 American Chemical Society

DOI: 10.1021/acs.joc.6b01838
J. Org. Chem. 2016, 81, 9775−9784

Scheme 1. Glorius Group's NHC-Catalyzed Formal [4 + 3] and [4 + 1] Annulation Reactions

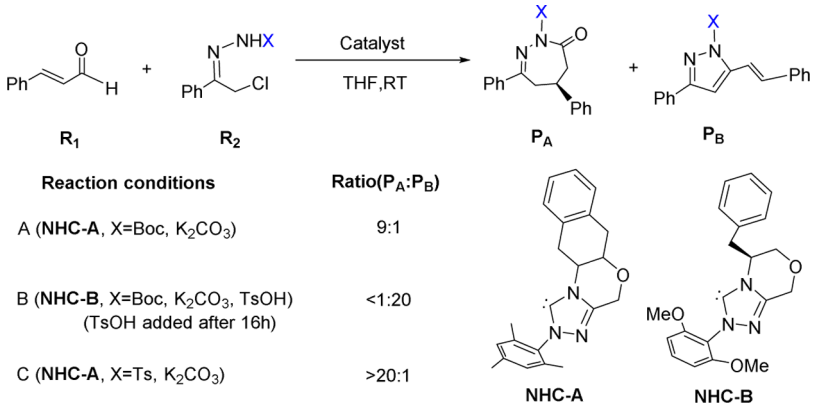

Scheme 2. Possible Reaction Mechanisms Proposed by the Glorius Group

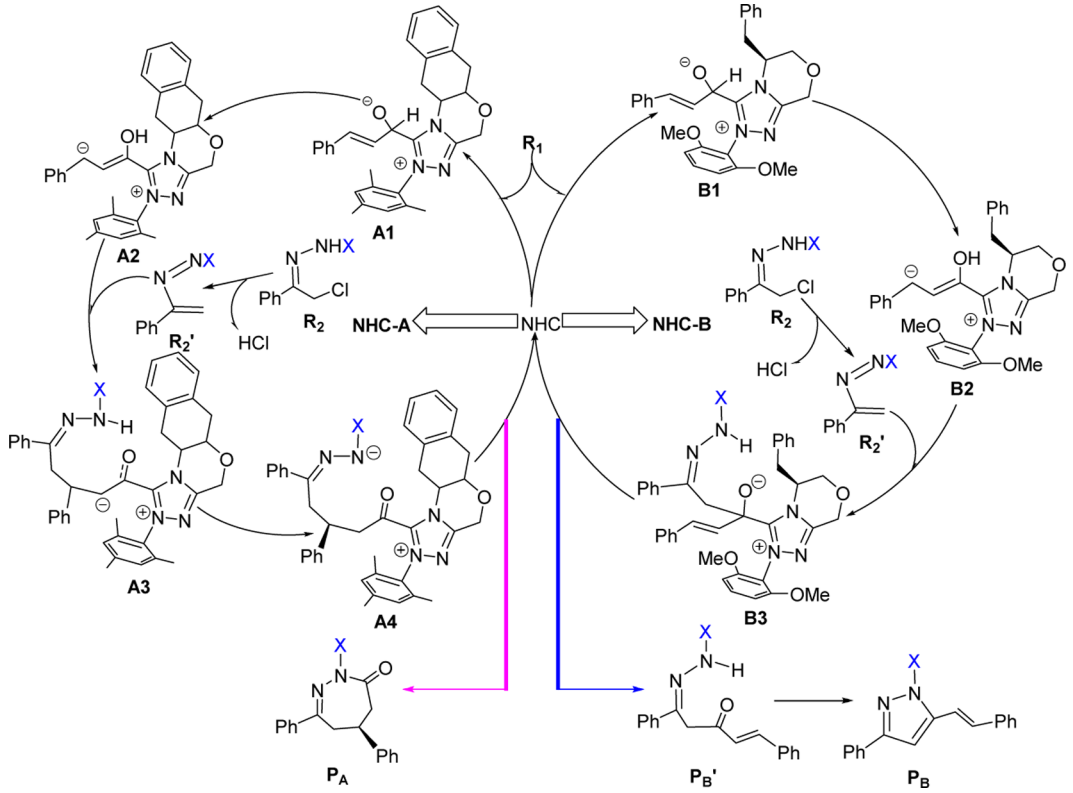

Finally, N-acylation reaction occurs to extrude the NHC catalyst and produce product $\mathbf{P_A}$. In the case of [4 + 1] annulation, dissociation of the NHC catalyst from **B3** generates intermediate product $\mathbf{P_B}'$, which then undergoes annulation via dehydration, producing final product $\mathbf{P_B}$.

A full understanding of the reaction mechanisms is still, to date, a major challenge for experimentalists as well as for theoreticians.[23] Although the plausible mechanistic pathway has been proposed by the Glorius group, some key issues still need to be further discussed. (1) How does the proton transfer occur in step **A1** → **A2** or **B1** → **B2**? (2) How is the origin of homoenolate versus acyl anion 1,4-addition? (3) How does the transformation of $\mathbf{P_B}'$ → $\mathbf{P_B}$ occur? (4) More importantly, how is the origin of the selectivity observed experimentally? To address these questions, a theoretical investigation for detailed reaction mechanisms is needed. Herein, we report our detailed density functional theory (DFT) calculations on the reaction mechanisms in order to gain insight into interesting experimental observations and distinct selectivity. We expect this work would help to understand the detailed mechanisms and design new related reactions.

■ COMPUTATIONAL DETAILS

All of the structures were optimized and characterized as energy minima (zero imaginary frequencies) or transition states (one imaginary frequencies) at the B3LYP[24−26]/6-31G(d,p) level. The electronic energies calculated were then improved by M06-2X[27,28]/6-311+G(d,p) single-point calculations, which took the solvent effects into account by using the SMD[29] solvent model. The thermal corrections for enthalpies and Gibbs free energies were carried out at 298.15 K and 1 atm by using B3LYP/6-31G(d,p) harmonic frequencies. Where necessary, intrinsic reaction coordinate[30,31] calculations were conducted in order to verify the transition states actually connecting the corresponding two minima. Unless otherwise stated, the Gibbs free energies calculated in THF solution (ΔG_{sol}) are used to discuss the energetic profiles presented in

DOI: 10.1021/acs.joc.6b01838
J. Org. Chem. 2016, 81, 9775−9784

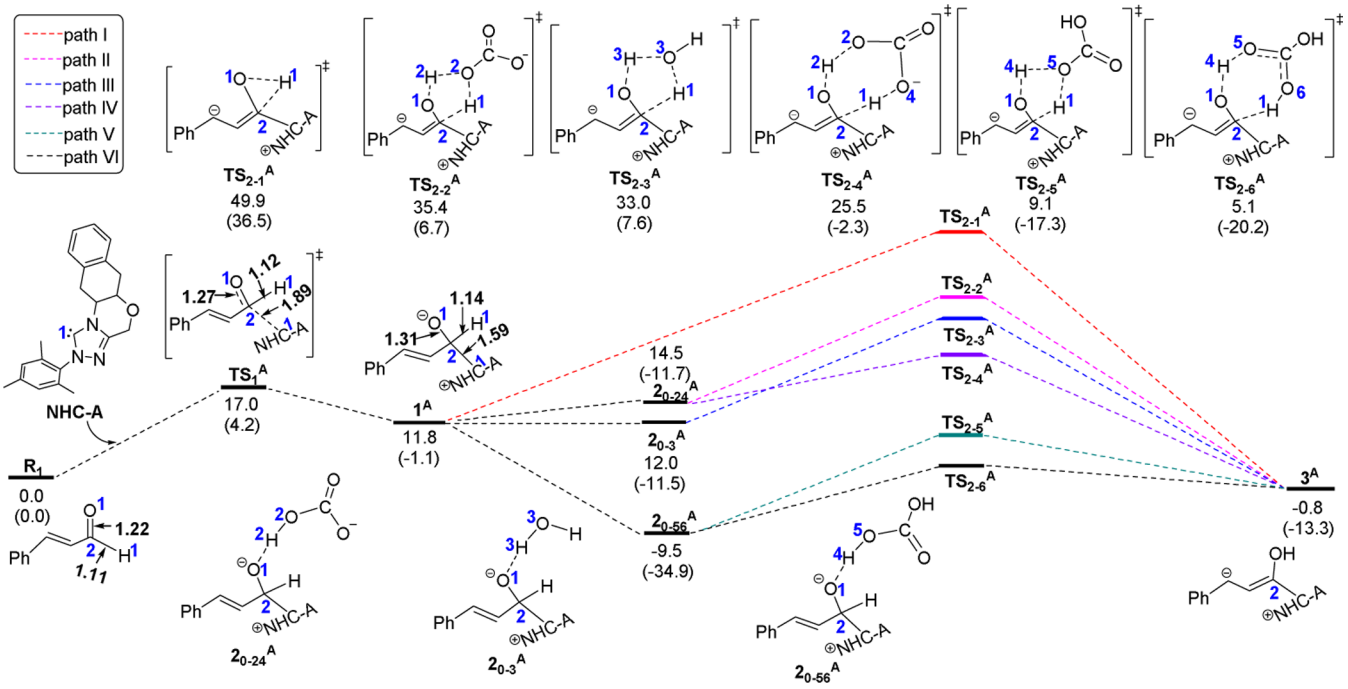

Figure 1. Free energy diagram for the reaction leading to Breslow intermediate 3^A catalyzed by **NHC-A**. The relative free energies and relative enthalpic energies (in parentheses) are given in kcal/mol. Bond distances are given in Å.

this work. All of the calculations were carried out with the Gaussian 09 package.[32]

RESULTS AND DISCUSSION

In this work, we first investigate the **NHC-A**-catalyzed [4 + 3] and [4 + 1] annulation mechanisms leading to 1,2-diazepines ($\mathbf{P_A}^{Boc}$) and pyrazoles ($\mathbf{P_B}^{Boc}$), respectively (reaction A). Then we study the reaction mechanisms catalyzed by **NHC-B** (reaction B) to probe the regioselectivity observed experimentally. Finally, we explore the influence of substituents on the regioselectivity of **NHC-A**-catalyzed [4 + 3] and [4 + 1] reactions (reaction C).

NHC-A-Catalyzed Reaction Mechanism. The free energy diagrams of **NHC-A**-catalyzed annulation reaction leading to $\mathbf{P_A}^{Boc}$ and $\mathbf{P_B}^{Boc}$ are calculated and shown in Figures 1, 3, and 4. Optimized structures of key transition states for proton transfer are presented in Figure 2.

In Figure 1, the reaction is initiated by nucleophilic attack of **NHC-A** at the carbonyl carbon of reactant $\mathbf{R_1}$ to afford a zwitterionic intermediate $\mathbf{1}^A$ via transition state $\mathbf{TS_1}^A$. The C1−C2 bond is shortened from 1.89 Å in $\mathbf{TS_1}^A$ to 1.59 Å in $\mathbf{1}^A$, indicating gradual formation of the C1−C2 bond. The low free energy barrier (17.0 kcal/mol) indicates that the nucleophilic addition is kinetically accessible. The less favored thermodynamics (11.8 kcal/mol) mainly results from the entropy decrease. As a result, the elongated C2−H1 bond together with the more nucleophilic O1 anion in $\mathbf{1}^A$ promotes the subsequent proton transfer.

In the following proton transfer process, H1 migrates as a proton to the anionic oxygen, delivering Breslow intermediate $\mathbf{3}^A$. Various proton transfer modes were considered in this study. Direct 1,2-proton transfer via a three-membered ring transition state $\mathbf{TS_{2-1}}^A$ is calculated to require a too high barrier (49.9 kcal/mol) (path I in Figure 1) as a result of strong ring strain. The calculated distances of H1···O1 and H1···C2 are 1.34 and 1.19 Å, respectively (Figure 2). Previous studies[33−37] have reported that trace water and the additive in the solvent could assist proton transfer. Thus, we considered water, bicarbonate, and carbonic acid acting as shuttles to promote the proton transfer. Note that the bicarbonate is actually generated with the HCl elimination from $\mathbf{R_2}$ (vide infra). Related calculated results are shown in Figure 1 (path III, water-assisted; paths II and IV, bicarbonate-assisted; paths V and VI, carbonic-acid-assisted).

In the H_2O-assisted proton transfer process, hydrogen bonding of $\mathbf{1}^A$ with water affords intermediate $\mathbf{2_{0-3}}^A$. Then proton transfer via $\mathbf{TS_{2-3}}^A$ occurs, leading to the hydroxyl intermediate $\mathbf{3}^A$ with a free energy barrier of 33.0 kcal/mol (see path III in Figure 1). For the proton transfer with HCO_3^- and H_2CO_3 acting as shuttles, the calculations predict that H_2CO_3 is preferable. The H_2CO_3-promoted proton transfer via the seven-center ring transition state $\mathbf{TS_{2-6}}^A$ just requires an activation energy of 14.6 kcal/mol ($\mathbf{2_{0-56}}^A \rightarrow \mathbf{TS_{2-6}}^A$) (see path VI in Figure 1), and that via a five-center ring transition state $\mathbf{TS_{2-5}}^A$ requires 18.6 kcal/mol ($\mathbf{2_{0-56}}^A \rightarrow \mathbf{TS_{2-5}}^A$) (see path V in Figure 1). Related bond distances and bond angles in $\mathbf{TS_{2-6}}^A$ are given in Figure 2. Maybe the C−O−C conjugation moiety involved in the seven-center ring transition state contributes to the relatively lower barrier.

Figure 3 presents the free energy profile for the path from $\mathbf{3}^A$ to product $\mathbf{P_A}^{Boc}$. Releasing a HCl molecule from reactant $\mathbf{R_2}^{Boc}$ gives $\mathbf{R_2}^{Boc'}$ to allow formation of the C7═C8 double bond. The HCl elimination mechanisms,[38] including the direct and the K_2CO_3-involved mechanisms, were calculated and are shown in Figure S1 in the Supporting Information. The calculated results indicated that the direct HCl elimination is unachievable due to significant instability of the elimination product. Instead, our calculations indicate that the additive K_2CO_3 indeed promotes the HCl elimination, making the process thermodynamically and kinetically accessible. The generated HCO_3^- can be used to facilitate the proton transfer as mentioned in Figure 1 and subsequent steps. The terminal C8 atom of $\mathbf{R_2}^{Boc'}$ is subject to nucleophilic attack of $\mathbf{3}^A$. As shown in this figure, $\mathbf{3}^A$ has two

DOI: 10.1021/acs.joc.6b01838
J. Org. Chem. 2016, 81, 9775−9784

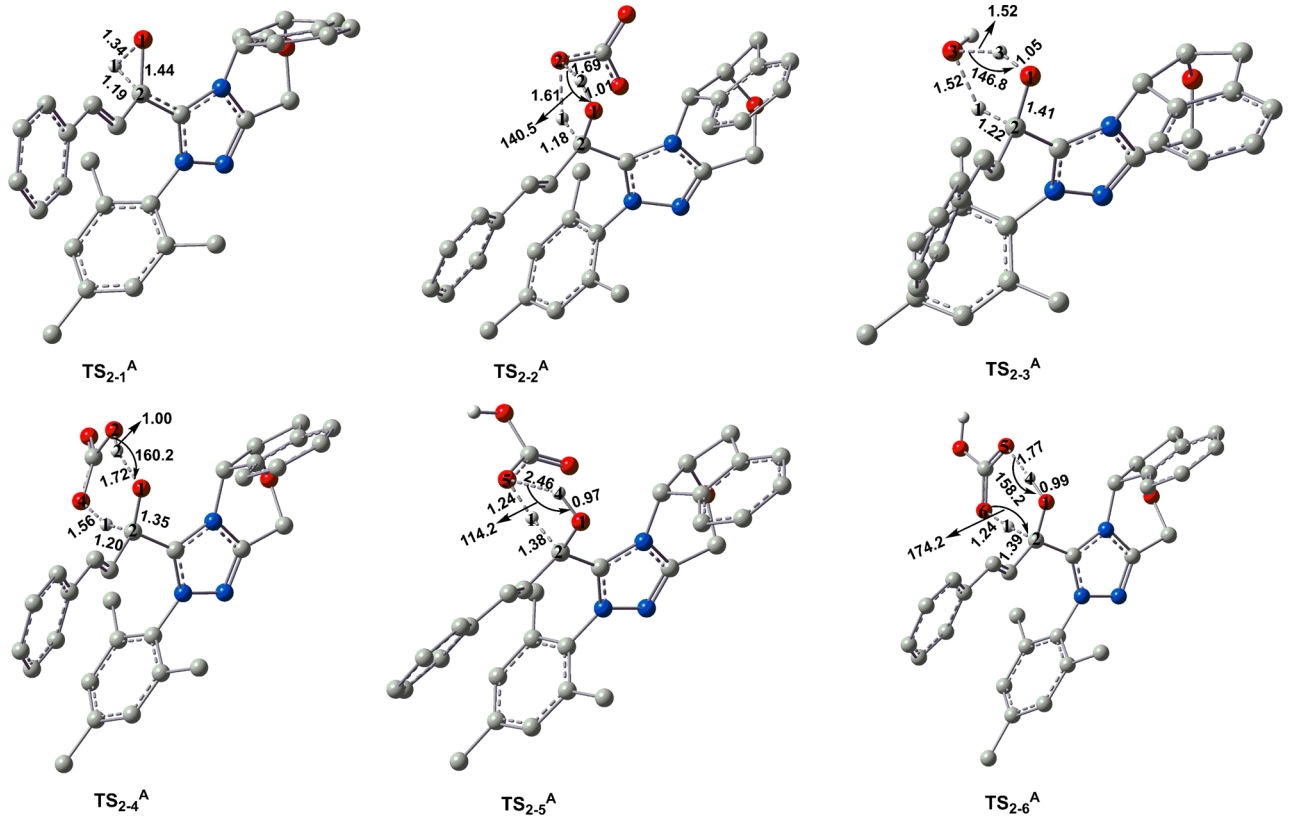

Figure 2. Optimized geometries of proton transfer transition states involved in Figure 1. The hydrogen atoms except for the transferring protons are omitted. Bond distances are given in Å, and bond angles are given in degrees.

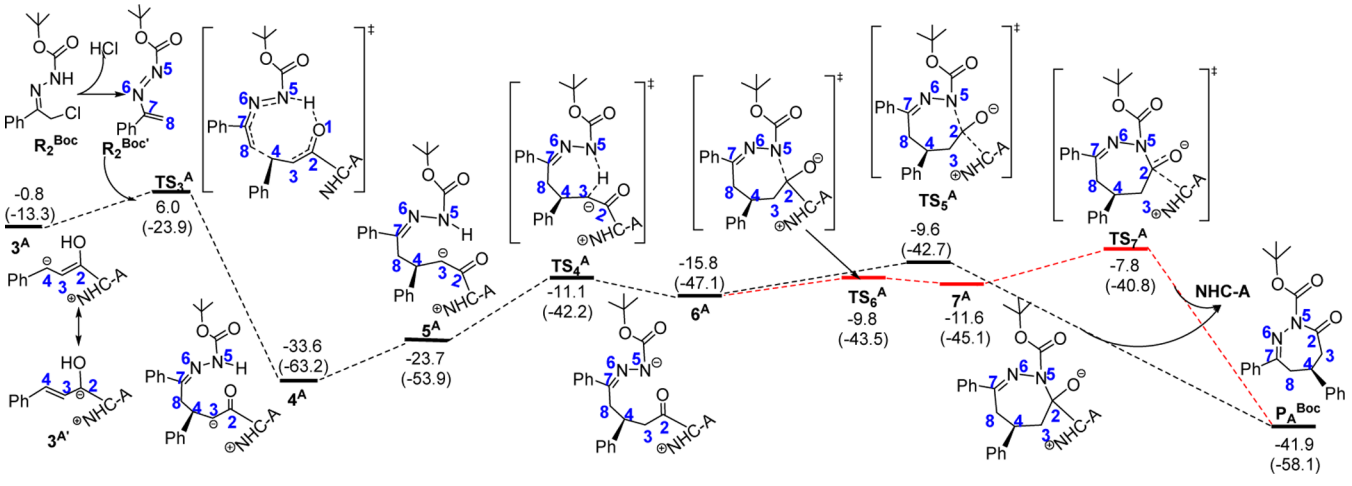

Figure 3. Free energy diagram calculated for reaction of 3^A with $R_2^{Boc'}$ leading to product P_A^{Boc}. The relative free energies and relative enthalpic energies (in parentheses) are given in kcal/mol.

resonance modes with one bearing a negative formal charge at C4 and the other at C2. In this section, nucleophilic attack of 3^A via C4 toward C8 of $R_2^{Boc'}$ was considered. This step affords intermediate 4^A involving two events: C4−C8 bond formation and concurrent proton transfer from O1 to N5. The nucleophilic addition is demonstrated by our calculations to be both kinetically and thermodynamically favored with a barrier of 6.8 kcal/mol and reaction energy of −32.8 kcal/mol. 4^A then isomerizes to intermediate 5^A, with C3 being proximate to N5, which becomes conducive to the subsequent proton transfer. The proton transfer from N5 to C3 generates intermediate 6^A via TS_4^A. Finally, nucleophilic addition of N5 to the carbonyl C2 is expected. Two competitive paths were proposed from 6^A to product P_A^{Boc}. One is a concerted cyclization (a one-step process), and the other is a stepwise one (a two-step process). In the concerted process, N5−C2 bond formation and **NHC-A** extrusion occur concurrently. In the stepwise process, the N5−C2 bond formation first occurs to give intermediate 7^A, and then **NHC-A** release is followed to produce the product P_A^{Boc}. As the calculated results indicated, the concerted TS_5^A is more stable than TS_7^A involved in the stepwise cyclization by 1.8 kcal/mol. Thus, the concerted cyclization is predicted to be preferred. The **NHC-A**-catalyzed cyclization reaction $R_1 + R_2^{Boc} \rightarrow P_A^{Boc}$ is predicted to overcome an overall activation barrier of 24.0 kcal/mol ($4^A \rightarrow TS^{5A}$).

DOI: 10.1021/acs.joc.6b01838
J. Org. Chem. 2016, 81, 9775−9784

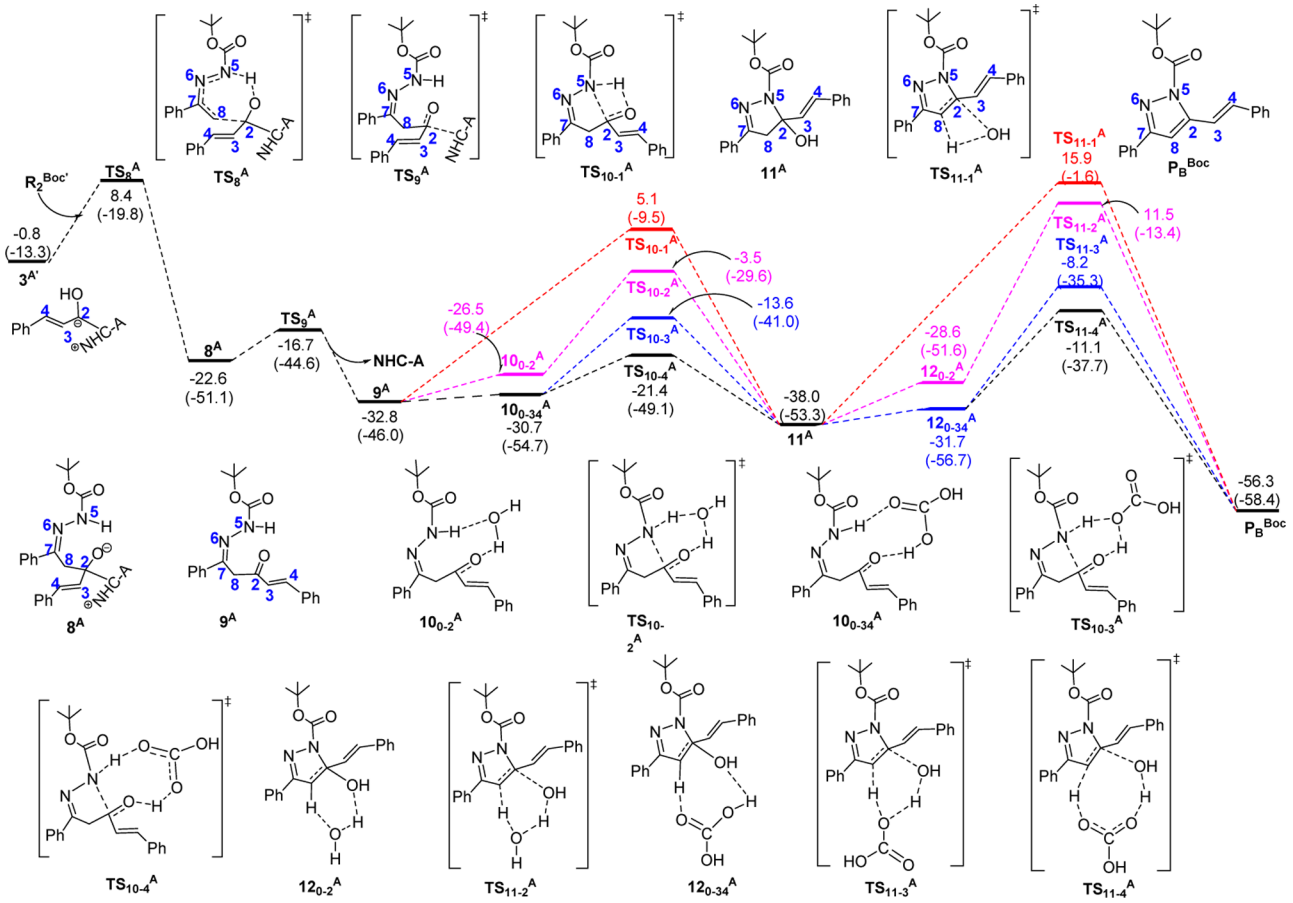

Figure 4. Free energy diagram calculated for the reaction of $3^{A\prime}$ with $R_2^{Boc\prime}$ leading to product P_A^{Boc}. The relative free energies and relative enthalpic energies (in parentheses) are given in kcal/mol.

Other possible pathways were also considered, for example, the pathway with H1 transferring to C3 in 1^A followed by reacting with $R_2^{Boc\prime}$. Calculated results indicated that such a proposal is inaccessible (see Figure S2 in Supporting Information). The inaccessible pathways initiated from **NHC-A** nucleophilic attack toward $R_2^{Boc\prime}$ were also calculated (see Figure S3 in Supporting Information).

As shown in Figure 4, $R_2^{Boc\prime}$ can also react with $3^{A\prime}$ (the homoenolate equivalent of Breslow intermediate 3^A) to produce the five-membered [4 + 1] product P_B^{Boc}. The C2 atom of $3^{A\prime}$ nucleophilically attacks the C8 atom of $R_2^{Boc\prime}$ via TS_8^A, leading to intermediate 8^A. This step requires an activation energy of 9.2 kcal/mol, and the formed intermediate 8^A is 21.8 kcal/mol lower than $3^{A\prime}$, indicating that 8^A is stable. Then, elimination of **NHC-A** from 8^A affords intermediate 9^A through TS_9^A. The 5.9 kcal/mol free energy barrier suggests that **NHC-A** is a good leaving group. In the following intramolecular cyclization and proton transfer process, the C2−N5 bond formation and proton transfer from N5 to the carbonyl oxygen occur simultaneously. We calculated the direct ($9^A \rightarrow TS_{10-1}^A \rightarrow 11^A$), H_2O-assisted ($9^A \rightarrow 10_{0-2}^A \rightarrow TS_{10-2}^A \rightarrow 11^A$), and H_2CO_3-assisted proton transfer ($9^A \rightarrow 10_{0-34}^A \rightarrow TS_{10-3}^A \rightarrow 11^A$ and $9^A \rightarrow 10_{0-34}^A \rightarrow TS_{10-4}^A \rightarrow 11^A$) processes. The free energy barriers corresponding to the above transformations are calculated to be 37.9, 29.3, 19.2, and 11.4 kcal/mol, indicating the H_2CO_3-assisted proton transfer is the most favored. Finally, 11^A is dehydrated to generate product P_B^{Boc}. The free energy barrier for the direct dehydration process ($11^A \rightarrow TS_{11-1}^A \rightarrow P_B^{Boc}$) is calculated to be as high as 53.9 kcal/mol, due to strong strain of the four-membered ring in TS_{11-1}^A. Hence, we studied the H_2O-assisted and H_2CO_3-assisted dehydration processes (see Figure 4). The calculated results suggest that the H_2CO_3-assisted dehydration step can occur in mild condition with the free energy barrier of 26.9 kcal/mol ($11^A \rightarrow TS_{11-4}^A$). Also, this process is found from Figure 4 to be rate-determining for the **NHC-A**-catalyzed [4 + 1] annulation leading to product P_B^{Boc}.

Examining the free energy diagrams shown in Figures 1, 3, and 4, one can see the **NHC-A**-catalyzed regioselectivity access to products P_A^{Boc} and P_B^{Boc} is determined by the relative stability of TS_3^A versus TS_8^A. The lower energy of TS_3^A is consistent with the experimental observations that P_A^{Boc} is obtained as the major product.

NHC-B-Catalyzed Reaction Mechanism. The free energy diagrams for the favored **NHC-B**-catalyzed mechanism leading to P_A^{Boc} are shown in Figure 5. The reaction includes five steps: nucleophilic addition of **NHC-B** to R_1, formation of Breslow intermediate 3^B (other possible proton transfer transition states are presented in Figure S4 in the Supporting Information), reaction of 3^B with $R_2^{Boc\prime}$, [4 + 3] cycloaddition, and release of **NHC-B**. The rate-determining step for the reaction is the nucleophilic attack of 3^B to $R_2^{Boc\prime}$ via TS_3^B with an overall barrier of 29.4 kcal/mol.

The free energy diagrams for the favored **NHC-B**-catalyzed mechanism leading to P_B^{Boc} are shown in Figure 6. The reaction includes five steps: nucleophilic addition of **NHC-B** to R_1, formation of homoenolate equivalent $3^{B\prime}$, reaction of $3^{B\prime}$ with $R_2^{Boc\prime}$, release of **NHC-B**, intramolecular cyclization concerted with proton transfer, and TsOH-assisted dehydration.

DOI: 10.1021/acs.joc.6b01838
J. Org. Chem. 2016, 81, 9775−9784

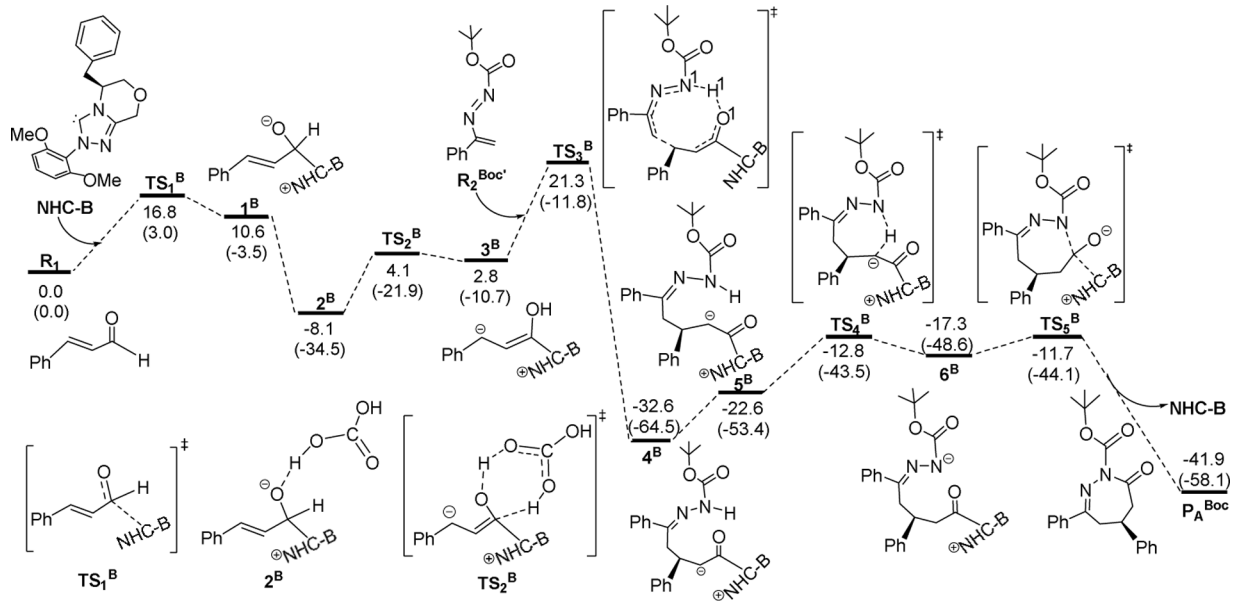

Figure 5. Free energy diagram calculated for the reaction of $\mathbf{R_1}$ with $\mathbf{R_2}^{\mathbf{Boc\prime}}$ leading to the product $\mathbf{P_A}^{\mathbf{Boc}}$ catalyzed by **NHC-B**. The relative free energies and relative enthalpic energies (in parentheses) are given in kcal/mol.

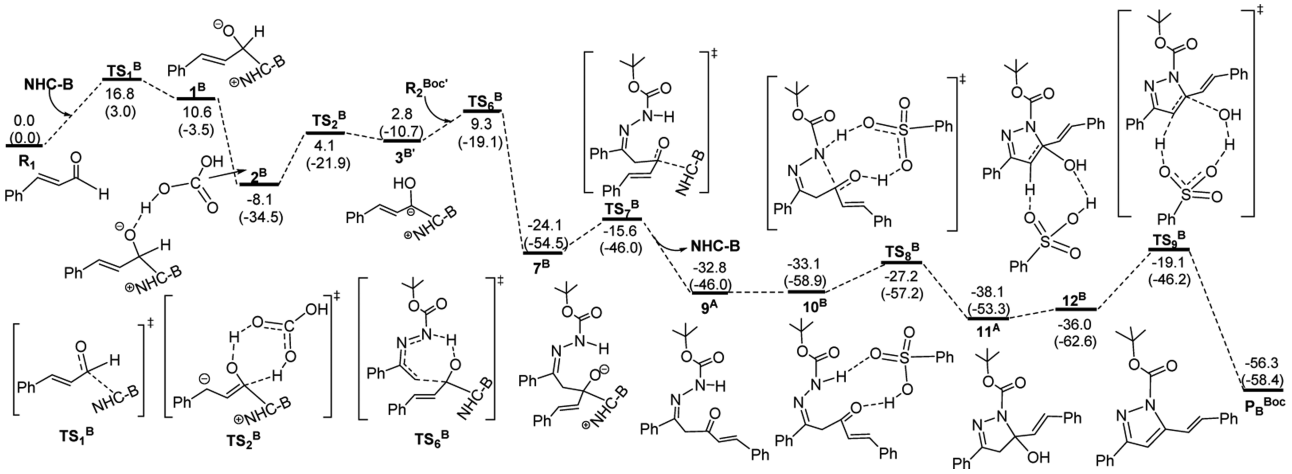

Figure 6. Free energy diagram calculated for **NHC-B**-catalyzed reaction of $\mathbf{R_1}$ with $\mathbf{R_2}^{\mathbf{Boc\prime}}$ leading to product $\mathbf{P_B}^{\mathbf{Boc}}$. The relative free energies and relative enthalpic energies (in parentheses) are given in kcal/mol.

The TsOH-assisted dehydration is calculated to be favored over the H_2O- and H_2CO_3-assisted processes (see Figures 4 and 6). The rate-determining step for the reaction is the dehydration step with an overall barrier of 19.0 kcal/mol. As shown in Figures 5 and 6, the **NHC-B**-catalyzed regioselectivity access to product $\mathbf{P_A}^{\mathbf{Boc}}$ versus $\mathbf{P_B}^{\mathbf{Boc}}$ is determined by relative stability of $\mathbf{TS_3}^{\mathbf{B}}$ versus $\mathbf{TS_6}^{\mathbf{B}}$. The lower barrier of $\mathbf{2}^{\mathbf{B}} \rightarrow \mathbf{TS_6}^{\mathbf{B}}$ is in good agreement with the experimental observations that $\mathbf{P_B}^{\mathbf{Boc}}$ is the major product.

Substituent Effect on the Reaction Mechanism. To explore the substituent influence on the regioselectivity for the **NHC-A**-catalyzed [4 + 3] and [4 + 1] annulation reactions, we also calculated the corresponding mechanisms when the substituent X in $\mathbf{R_2}$ is Ts (Figures 7 and 8).

The favored mechanism for the **NHC-A**-catalyzed [4 + 3] annulation reactions with Ts and Boc as respective substituent diverges from Breslow intermediate $\mathbf{3}^{\mathbf{A}}$. Five steps are also involved in the reaction as mentioned above. The overall free energy barrier for the reaction with Ts as the substituent is associated with the **NHC-A** leaving and calculated to be 20.1 kcal/mol.

The favored free energy diagram for the **NHC-A**-catalyzed [4 + 1] annulation reaction with Ts as the substituent is calculated and shown in Figure 8. The reaction includes five steps: nucleophilic addition of **NHC-A** to $\mathbf{R_1}$, formation of homoenolate equivalent $\mathbf{3}^{\mathbf{A\prime}}$, reaction of $\mathbf{3}^{\mathbf{A\prime}}$ with $\mathbf{R_2}^{\mathbf{Ts\prime}}$, **NHC-A** leaving, intramolecular cyclization concerted with proton transfer (other possible proton transfer transition states are listed in Figure S5 in the Supporting Information), and dehydration (other possible dehydration transition states are listed in Figure S5 in the Supporting Information). The rate-determining step for the reaction is the dehydration step, and the overall free energy barrier is 26.2 kcal/mol.

As shown in Figures 7 and 8, the **NHC-A**-catalyzed regioselectivity for product $\mathbf{P_A}^{\mathbf{Ts}}$ versus $\mathbf{P_B}^{\mathbf{Ts}}$ is determined by the energy difference between $\mathbf{TS_3}^{\mathbf{C}}$ and $\mathbf{TS_6}^{\mathbf{C}}$. The lower relative energy of $\mathbf{TS_3}^{\mathbf{C}}$ is in agreement with the experimental observations that $\mathbf{P_A}^{\mathbf{Ts}}$ is the major product.

DOI: 10.1021/acs.joc.6b01838
J. Org. Chem. 2016, 81, 9775−9784

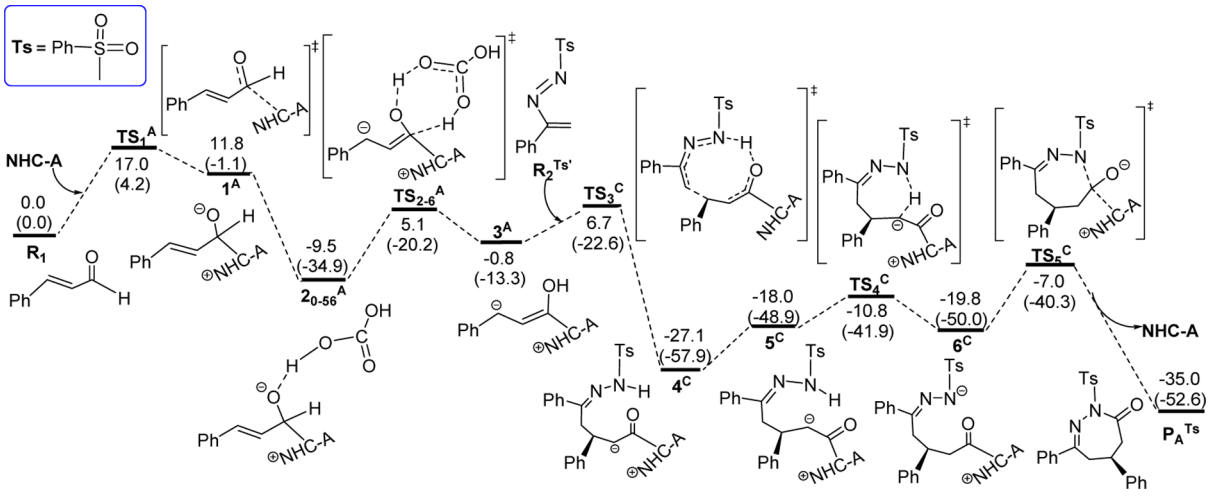

Figure 7. Free energy diagram calculated for the reaction of $\mathbf{R_1}$ with $\mathbf{R_2}^{Ts\prime}$ leading to the product $\mathbf{P_A}^{TS}$ catalyzed by **NHC-A**. The relative free energies and relative enthalpic energies (in parentheses) are given in kcal/mol.

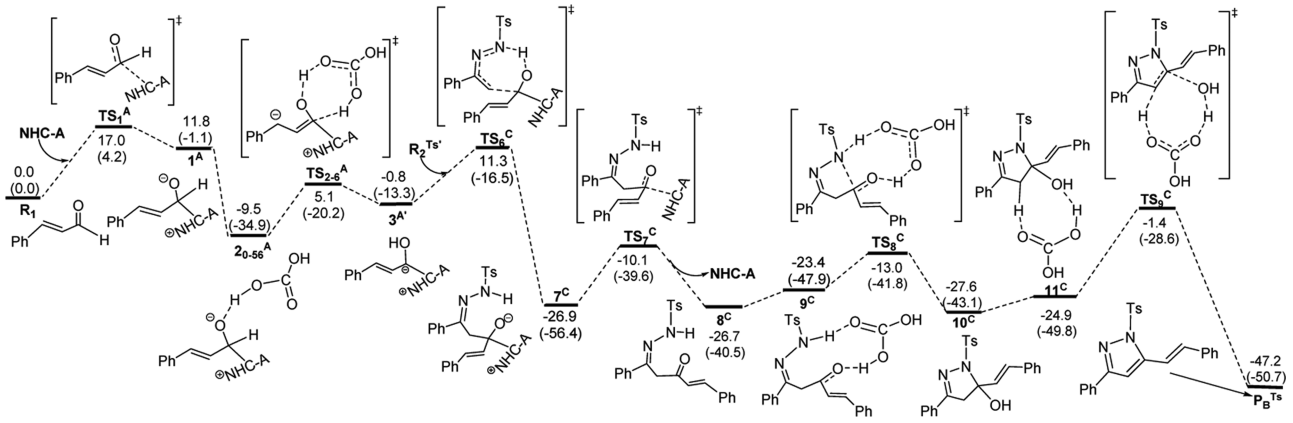

Figure 8. Free energy diagram calculated for the reaction of $\mathbf{R_1}$ with $\mathbf{R_2}^{Ts\prime}$ leading to the product $\mathbf{P_B}^{TS}$ catalyzed by **NHC-A**. The relative free energies and relative enthalpic energies (in parentheses) are given in kcal/mol.

Table 1. Regioselectivity-Determining and Rate-Determining Steps in Reactions A, B, and C, with Related Reaction Energies and Activation Energies (kcal/mol)

reactions	annulation types	regioselectivity-determining step, ΔG_1[a] and $\Delta G_1^{\ddagger}$[b]			rate-determining step ($\Delta G_2^{\ddagger}$)[c]
NHC-A-catalyzed[d] (reaction A)	[4 + 3]	$\mathbf{3}^{A}$ + $\mathbf{R_2}^{Boc\prime}$	−32.8	6.8	concerted cyclization (24.0)
	[4 + 1]	$\mathbf{3}^{A\prime}$ + $\mathbf{R_2}^{Boc\prime}$	−21.8	9.2	H_2CO_3-assisted dehydration (26.9)
NHC-B-catalyzed[e] (reaction B)	[4 + 3]	$\mathbf{3}^{B}$ + $\mathbf{R_2}^{Boc\prime}$	−35.3	18.5	[4 + 3] cycloaddition (29.4)
	[4 + 1]	$\mathbf{3}^{B\prime}$ + $\mathbf{R_2}^{Boc\prime}$	−26.8	6.5	TsOH-assisted dehydration (19.0)
NHC-A-catalyzed (reaction C)	[4 + 3]	$\mathbf{3}^{A}$ + $\mathbf{R_2}^{Ts\prime}$	−26.3	7.5	concerted cyclization (20.1)
	[4 + 1]	$\mathbf{3}^{A\prime}$ + $\mathbf{R_2}^{Ts\prime}$	−26.1	12.1	H_2CO_3-assisted dehydration (26.2)

[a] ΔG_1, reaction energy of **3** and $\mathbf{R_2}'$. [b] $\Delta G_1^{\ddagger}$, Gibbs free activation energy of **3** and $\mathbf{R_2}'$. [c] $\Delta G_2^{\ddagger}$, Gibbs free activation energy of rate-determining step. [d] $\mathbf{3}^{A\prime}$ is the resonance form of $\mathbf{3}^{A}$. [e] $\mathbf{3}^{B\prime}$ is the resonance form of $\mathbf{3}^{B}$.

In order to give a clear picture, the mechanistic scenarios for reactions A, B, and C are summarized in Table 1. For reactions A, B, and C, the regioselectivity-determining steps together with their reaction energies and activation energies are presented. Also, the rate-determining steps involved in the three reactions together with their activation energies are also listed. It can be seen from the table that [4 + 3] and [4 + 1] annulations diverge from the reaction of **3** and $\mathbf{R_2}'$, and reaction of **3** and $\mathbf{R_2}'$ is the regioselectivity-determining step for all of the reactions. This step is much favored thermodynamically as proven by the ΔG_1 values in the table. Examining the activation energies of the reverse reactions of **3** and $\mathbf{R_2}'$ from preceding energy diagrams, one can see that all of the reverse reactions are unachievable kinetically with too high activation energies. Consequently, it is predictive that reactions of **3** and $\mathbf{R_2}'$ are irreversible, and thus this divergent step determines the product ratio of [4 + 3] versus [4 + 1] annulations. The product ratio value is determined by the relative stability of the two divergent transition states from reaction of **3** + $\mathbf{R_2}'$. One is associated with [4 + 3] annulation and the other with [4 + 1] annulation.

For **NHC-A**-catalyzed reaction A, reaction of **3** + $\mathbf{R_2}'$ for [4 + 3] annulation is calculated to be kinetically more favored than that for [4 + 1] annulation. The rate-determining steps are predicted to be in the last stage of the two reactions (the concerted

DOI: 10.1021/acs.joc.6b01838
J. Org. Chem. 2016, 81, 9775−9784

Table 2. Distortion/Interaction Analysis for the R_2' Addition Transition States[a]

TS	$\Delta G^{\ddagger}$	$\Delta E^{\ddagger}_{dist}(3)$[b]	$\Delta E^{\ddagger}_{dist}(R_2')$[c]	$\Delta E^{\ddagger}_{dist}(3) + \Delta E^{\ddagger}_{dist}(R_2')$	$\Delta E^{\ddagger}_{int}$[d]	$\Delta E^{\ddagger}$
TS_3^A	6.8	5.2	9.7	14.9	−25.4	−10.5
TS_8^A	9.2	3.6	11.5	15.1	−21.9	−6.8
TS_3^B	18.5	11.0	9.8	20.8	−20.9	−0.1
TS_6^B	6.5	0.0	8.7	8.7	−17.7	−9.0
TS_3^C	7.5	4.0	8.7	12.7	−22.3	−9.6
TS_6^C	12.1	5.2	11.0	16.2	−20.2	−4.0

[a]Energies are given in kcal/mol. [b]Energy to distort intermediate **3** to transition state geometry. [c]Energy to distort reactant R_2' to transition state geometry. [d]Energy of interaction between the distorted intermediate **3** and reactant R_2' in the transition state.

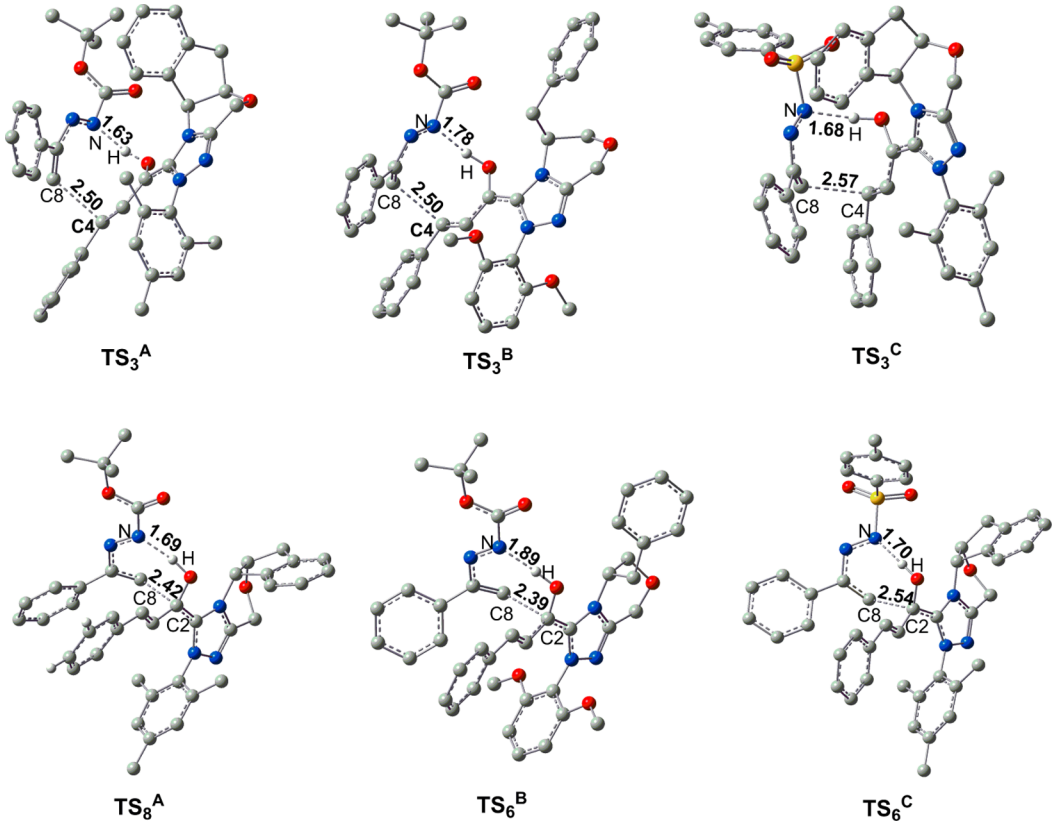

Figure 9. Optimized geometries of the R_2 addition transition states. The hydrogen atoms which are not involved in the reaction are omitted. Bond distances are given in Å.

cyclization process for [4 + 3] annulation, and the H_2CO_3-assisted dehydration process for [4 + 1] annulation). For **NHC-B**-catalyzed reaction B, the activation energy for reaction of **3** + R_2' leading to [4 + 3] annulation is increased to as high as 18.5 kcal/mol, and this step becomes the rate-determining step. In the [4 + 1] annulation, reaction of **3** + R_2' proceeds smoothly with a low barrier of 6.5 kcal/mol, and the rate-determining step is still in the last stage of the whole reaction (the TsOH-assisted dehydration process). For **NHC-A**-catalyzed reaction C with Ts as the substituent, a similar situation with reaction A is found, but the activation energy difference between the two reactions of **3** + R_2' is enlarged (4.6 kcal/mol) as compared to the one in reaction A (2.4 kcal/mol).

Origin of the Regioselectivity. To gain insight into origin of the observed regioselectivity, distortion−interaction analyses for the R_2' addition transition states (TS_3^A, TS_8^A, TS_3^B, TS_6^B, TS_3^C, and TS_6^C) are performed.[39] The energies required to distort the intermediate **3** and reactant R_2' into the geometries of corresponding transition states, $\Delta E^{\ddagger}_{dist}(3)$ and $\Delta E^{\ddagger}_{dist}(R_2')$, respectively, are given in Table 2. The distortion energy of $\Delta E^{\ddagger}_{dist}(3)$ is defined as the energy difference between the ground state of **3** and the distorted **3** in the transition state geometry, and the distortion energy of $\Delta E^{\ddagger}_{dist}(R_2')$ is that between the ground state of R_2' and the distorted R_2' in the transition state geometry. $\Delta E^{\ddagger}_{int}$[d], representing the interaction energy between distorted **3** and distorted R_2', is also listed in Table 2. Optimized structures of the six R_2' addition transition states are presented in Figure 9.

In reaction A with **NHC-A** as the catalyst, we compare the pair of TS_3^A and TS_8^A that determine the regioselectivity leading to P_A^{Boc} and P_B^{Boc}. It can be seen from Table 2 that the total distortion energy involved in both transition states are close ($\Delta E^{\ddagger}_{dist}(3) + \Delta E^{\ddagger}_{dist}(R_2')$, 14.9 vs 15.1 kcal/mol), while the interaction energy is different ($\Delta E^{\ddagger}_{int}$[d], −25.4 vs −21.9 kcal/mol). Clearly, stronger interaction energy involved in TS_3^A is responsible for its higher stability as compared to TS_8^A. As indicated in the geometries of the two transition states, the N···H interaction in TS_3^A (1.63 Å) is stronger than that in TS_8^A (1.69 Å), supporting our above prediction. Consistently, TS_3^A is found to be earlier

DOI: 10.1021/acs.joc.6b01838
J. Org. Chem. 2016, 81, 9775−9784

than TS_8^A with the C···C distance longer in the former than in the latter. Calculations show that C4···C8 is 2.50 Å in TS_3^A and C2···C8 is 2.42 Å in TS_8^A. In summary, stronger interaction between **3** and R_2' in TS_3^A may be the main reason leading to P_A^{Boc} as the major product.

In reaction B with **NHC-B** as the catalyst, the total distortion energy difference involved in TS_6^B and TS_3^B is 8.7−20.8 = −12.1 kcal/mol, while the interaction energy difference of distorted **3** and distorted R_2' is (−17.7) − (−20.9) = 3.2 kcal/mol. Thus, one can deduce that less stability of TS_3^B is a result of the total remarkable distortion. Further examination from Table 2 demonstrates that the major structural distortion arises from distortion of **3** in TS_3^B. The distortion energy of **3** in TS_3^B is 11.0 kcal/mol, but nondistortion of **3** is found in TS_6^B (0.0 kcal/mol). Thus, we predict that strong structural distortion of **3** in TS_3^B switches the regioselectivity in comparison with reaction A, leading to P_B^{Boc} instead of P_A^{Boc} as the major product. The origin for the reversed regioselectivity can be explored as follows. Carefully examining the six-membered ring geometry of **NHC-B**, we found that a boat-type conformation exists in TS_3^B and a chair-type conformation in TS_6^B. The two conformations were extracted from both transition structures and saturated with hydrogen atoms, giving the structures as shown Figure S6 in the Supporting Information. Single-point calculations demonstrate that the boat-type conformation is less stable by 7.6 kcal/mol than the chair-type conformation in electronic energy, suggesting a major contribution to the electronic energy difference between TS_3^B and TS_6^B (8.9 kcal/mol). Optimization of the boat-type conformation directly turns into the chair-type conformation, implying the free boat-type conformation is not a stationary point but can be present in the structure of TS_3^B. We conclude that employment of **NHC-B** forces the catalyst to adopt a relatively unstable boat-type conformation in TS_3^B, resulting in strong structural distortion of **NHC-B** and thus making the transition state less stable as compared with TS_6^B that involves a chair-type conformation of **NHC-B**. Therefore, the product formed via TS_6^B becomes the major product, in accordance with the experimental facts.

In reaction C, in comparison with TS_6^C, TS_3^C involves small distortion energy and larger interaction energy. Therefore, the product P_A^{Ts} via TS_3^C is predicted to be the major product, consistent with the experimental facts. The smaller distortion energy (12.7 kcal/mol) in TS_3^C of reaction C as compared to that (14.9 kcal/mol) in TS_3^A of reaction A leads to reaction C having a higher regioselectivity.

CONCLUSIONS

The NHC-catalyzed [4 + 3] and [4 + 1] annulations of enals with azoalkenes have been theoretically investigated with the aid of DFT calculations. Three reactions are included in this study, reaction A (**NHC-A** as the catalyst and Boc as the substituent), reaction B (**NHC-B** as the catalyst and Boc as the substituent), and reaction C (**NHC-A** as the catalyst and Ts as the substituent). Based one our mechanistic study, the additives used in the experiment are proven to play an important role in promoting proton transfer and dehydration steps. The regioselectivity for the three reactions is determined by the homoenolate 1,4-addition versus acyl anion 1,4-addition. The origin of regioselectivity is explored by performing the distortion−interaction analysis. In reaction A, [4 + 3] annulation is preferred mainly due to the stronger interaction energy between **3** and R_2' in TS_3^A. The reaction rate-determining step is predicted to be the last step, that is, the concerted cyclization step. In reaction B, [4 + 1] annulation is preferred over the [4 + 3] annulation mainly because there exists a large distortion energy of **3** in TS_3^B in the [4 + 3] annulation. Further analysis found that in the [4 + 3] annulation the large distortion energy of **3** in TS_3^B arises from formation of an unstable boat-type conformation involved in the **NHC-B** moiety. While TS_6^B leads to [4 + 1] annulation, a stable chair-type conformation is found to be present, leading to [4 + 1] annulation being kinetically more favorable. The TsOH-assisted dehydration in the last stage of the whole [4 + 1] annulation reaction is predicted to be the rate-determining step. In reaction C, smaller distortion energies of **3** and R_2' in TS_3^C relative to those in TS_6^C, caused by employment of the Ts group, enlarge the activation energy gap between the two transition states and leads to [4 + 3] annulation more favored when compared to reaction A. The in-depth understanding for the divergent reaction mechanisms and distinct regiochemistry could be beneficial in designing new related reactions.

ASSOCIATED CONTENT

Supporting Information

The Supporting Information is available free of charge on the ACS Publications website at DOI: 10.1021/acs.joc.6b01838.

Complete ref 32 and tables giving all computed Cartesian coordinates (PDF)

Molecule coordinates (XYZ)

AUTHOR INFORMATION

Corresponding Author

*E-mail: siweibi@126.com.

Notes

The authors declare no competing financial interest.

ACKNOWLEDGMENTS

This work was jointly supported by National Natural Science Foundation of China (Nos. 21303073 and 21473100) and Talent Team Culturing Plan for Leading Disciplines of University in Shandong Province.

REFERENCES

(1) Michelini, S.; Cassano, G. B.; Frare, F.; Perugi, G. *Pharmacopsychiatry* **1996**, *29*, 127−134.

(2) Chakraborty, S.; Shah, N. H.; Fishbein, J. C.; Hosmane, R. S. *Bioorg. Med. Chem. Lett.* **2011**, *21*, 756−759.

(3) Antonow, D.; Thurston, D. E. *Chem. Rev.* **2011**, *111*, 2815−2864.

(4) Bondock, S.; Fadaly, W.; Metwally, M. A. *Eur. J. Med. Chem.* **2010**, *45*, 3692−3701.

(5) Bonesi, M.; Loizzo, M. R.; Statti, G. A.; Michel, S.; Tillequin, F.; Menichini, F. *Bioorg. Med. Chem. Lett.* **2010**, *20*, 1990−1993.

(6) Abdel-Aziz, M.; Abuo-Rahma, G. E. -D. A.; Hassan, A. A. *Eur. J. Med. Chem.* **2009**, *44*, 3480−3487.

(7) Liu, T.; Han, S. M.; Han, L. L.; Wang, L.; Cui, X. Y.; Du, C. Y.; Bi, S. W. *Org. Biomol. Chem.* **2015**, *13*, 3654−3661.

(8) Dünkelmann, P.; Kolter-Jung, D.; Nitsche, A.; Demir, A. S.; Siegert, P.; Lingen, B.; Baumann, M.; Pohl, M.; Müller, M. *J. Am. Chem. Soc.* **2002**, *124*, 12084−12085.

(9) Demir, A. S.; Sesenoglu, ö.; Dünkelmann, P.; Müller, M. *Org. Lett.* **2003**, *5*, 2047−2050.

(10) Cohen, D. T.; Scheidt, K. A. *Chem. Sci.* **2012**, *3*, 53−57.

(11) DiRocco, D. A.; Noey, E. L.; Houk, K. N.; Rovis, T. *Angew. Chem.* **2012**, *124*, 2441−2444.

(12) Sohn, S. S.; Rosen, E. L.; Bode, J. W. *J. Am. Chem. Soc.* **2004**, *126*, 14370−14371.

(13) Burstein, C.; Glorius, F. *Angew. Chem., Int. Ed.* **2004**, *43*, 6205−6208.

DOI: 10.1021/acs.joc.6b01838
J. Org. Chem. 2016, 81, 9775−9784

(14) Nair, V.; Babu, B. P.; Vellalath, S.; Suresh, E. *Chem. Commun.* **2008**, 747−749.
(15) Struble, J. R.; Kaeobamrung, J.; Bode, J. W. *Org. Lett.* **2008**, *10*, 957−960.
(16) Zhang, Y. R.; He, L.; Wu, X.; Shao, P. L.; Ye, S. *Org. Lett.* **2008**, *10*, 277−280.
(17) Huang, X. L.; Chen, X. Y.; Ye, S. *J. Org. Chem.* **2009**, *74*, 7585−7587.
(18) Lv, H.; Chen, X. Y.; Sun, L. H.; Ye, S. *J. Org. Chem.* **2010**, *75*, 6973−6976.
(19) Fu, Z. Q.; Sun, H.; Chen, S. J.; Tiwari, B.; Li, G. H.; Chi, Y. R. *Chem. Commun.* **2013**, *49*, 261−263.
(20) Izquierdo, J.; Orue, A.; Scheidt, K. A. *J. Am. Chem. Soc.* **2013**, *135*, 10634−10637.
(21) Lv, H.; Jia, W. Q.; Sun, L. H.; Ye, S. *Angew. Chem.* **2013**, *125*, 8769−8772.
(22) Guo, C.; Sahoo, B.; Daniliuc, C. G.; Glorius, F. *J. Am. Chem. Soc.* **2014**, *136*, 17402−17405.
(23) Yang, Y. F.; Shi, T.; Zhang, X. H.; Tang, Z. X.; Wen, Z. Y.; Quan, J. M.; Wu, Y. D. *Org. Biomol. Chem.* **2011**, *9*, 5845−5855.
(24) Becke, A. D. *J. Chem. Phys.* **1993**, *98*, 5648−5652.
(25) Lee, C. T.; Yang, W. T.; Parr, R. G. *Phys. Rev. B: Condens. Matter Mater. Phys.* **1988**, *37*, 785−789.
(26) Stephens, P. J.; Devlin, F. J.; Chabalowski, C. F.; Frisch, M. J. *J. Phys. Chem.* **1994**, *98*, 11623−11627.
(27) (a) Zhao, Y.; Truhlar, D. G. *Theor. Chem. Acc.* **2008**, *120*, 215−241. (b) Zhao, Y.; Truhlar, D. G. *Acc. Chem. Res.* **2008**, *41*, 157−167.
(28) (a) Lopez, S. A.; Houk, K. N. *J. Org. Chem.* **2013**, *78*, 1778−1783. (b) Lopez, S. A.; Munk, M. E.; Houk, K. N. *J. Org. Chem.* **2013**, *78*, 1576−1582. (c) Breugst, M.; Eschenmoser, A.; Houk, K. N. *J. Am. Chem. Soc.* **2013**, *135*, 6658−6668. (d) Qiao, Y.; Wei, D. H.; Chang, J. B. *J. Org. Chem.* **2015**, *80*, 8619−8630.
(29) Marenich, A. V.; Cramer, C. J.; Truhlar, D. G. *J. Phys. Chem. B* **2009**, *113*, 6378−6396.
(30) Fukui, K. *J. Phys. Chem.* **1970**, *74*, 4161−4163.
(31) Fukui, K. *Acc. Chem. Res.* **1981**, *14*, 363−368.
(32) Frisch, M. J.; et al. *Gaussian 09*, revision A.02; Gaussian, Inc.: Wallingford, CT, 2009. The full citation and computational details are given in the Supporting Information.
(33) Xia, Y. Z.; Liang, Y.; Chen, Y. Y.; Wang, M.; Jiao, L.; Huang, F.; Liu, S.; Li, Y. H.; Yu, Z. X. *J. Am. Chem. Soc.* **2007**, *129*, 3470−3471.
(34) Shi, F. Q.; Li, X.; Xia, Y. Z.; Zhang, L. M.; Yu, Z. X. *J. Am. Chem. Soc.* **2007**, *129*, 15503−15512.
(35) Liang, Y.; Zhou, H. L.; Yu, Z. X. *J. Am. Chem. Soc.* **2009**, *131*, 17783−17785.
(36) Mercier, E.; Fonovic, B.; Henry, C.; Kwon, O.; Dudding, T. *Tetrahedron Lett.* **2007**, *48*, 3617−3620.
(37) Zhao, L. L.; Wen, M. W.; Wang, Z. X. *Eur. J. Org. Chem.* **2012**, *2012*, 3587−3597.
(38) Zhao, L. L.; Chen, X. Y.; Ye, S.; Wang, Z. X. *J. Org. Chem.* **2011**, *76*, 2733−2743.
(39) Liu, P.; McCarren, P.; Cheong, P. H.-Y.; Jamison, T. F.; Houk, K. N. *J. Am. Chem. Soc.* **2010**, *132*, 2050−2057.

DOI: 10.1021/acs.joc.6b01838
J. Org. Chem. 2016, 81, 9775−9784